Polymer Chemistry

ROYAL SOCIETY OF CHEMISTRY

PAPER

View Article Online
View Journal | View Issue

Cite this: *Polym. Chem.*, 2024, **15**, 3311

Chemical doping-assisted shape transformation of block copolymer particles†

Zhengping Tan,‡[a] Jinseok Park, ‡[a] Sang Hoon Han,[a] Tan Ngoc-Lan Phan,[a] Younghyeon Ahn,[a] Meng Xu,[a] Shin-Hyun Kim, [a] Jaeman J. Shin *[b] and Bumjoon J. Kim *[a]

Received 15th May 2024,
Accepted 23rd July 2024

DOI: 10.1039/d4py00524d

rsc.li/polymers

Shape-tunable block copolymer (BCP) particles have attracted significant attention due to their applications as smart materials. Herein, we report iodine (I_2)-mediated doping of polystyrene-*block*-polybutadiene (PS-*b*-PB) particles as a facile strategy to transform spherical BCP particles into nonspherical shaped particles. Upon introducing the I_2 molecules to internally phase-separated spherical PS-*b*-PB particles, I_2 selectively reacts with the double bonds in PB blocks while leaving the PS block unaffected. Monitoring the shape-transformation process reveals a gradual structural transition from spheres to oblates and ellipsoids as a function of reaction time, consistent with the increasing conversion of the double bonds into I_2-doped cation radicals. Consequently, the interfacial tension of I_2-doped PB blocks decreases, neutralizing the interfacial interaction of BCP and its surroundings, thereby restructuring the spherical particles into shape-anisotropic forms. Furthermore, the versatility of I_2-mediated shape transition is demonstrated by applying the same chemistry to polystyrene-*block*-poly(4-vinylpyridine) BCP particles. Finally, spheroidal particles doped with I_2 exhibit photothermal heating behavior, highlighting their potential application as photothermal agents.

Introduction

Colloidal polymer particles with controlled shapes and well-defined internal structures have attracted significant attention due to their unique shape-dependent physical and optical properties.[1–4] Confined self-assembly of block copolymers (BCPs) in evaporative oil-in-water emulsions has been adopted as a robust and versatile method for producing anisotropic polymeric particles.[5–9] In this approach, the BCP droplets act as soft and mobile templates that undergo spontaneous deformation driven by the minimization of interfacial energy and chain stretching/bending penalty.[10,11] Recently, extensive efforts have been made to develop responsive BCP particles capable of shape transformation in response to external stimuli such as temperature, pH, or light.[12–19] In these systems, BCP particles undergo a reversible transition from spheres to ellipsoids or oblates under external stimuli, and this capability establishes controllable shape-dependent physicochemical properties. Consequently, these smart BCP particles hold promise for a range of potential applications as smart nanomaterials including sensors, detection, and coating.[20,21]

Surfactant engineering stands out as the most widely adopted strategy for generating nonspherical BCP particles by controlling the interfacial interaction between BCPs and the surrounding medium.[10,22–26] The key to this strategy lies in the precise selection or design of dual surfactants that favorably interact with a specific BCP domain, allowing for tunable interfacial tensions between each block and the aqueous surrounding through a mixture of surfactants. Accordingly, a neutral wetting condition between the BCPs and the surrounding media can be established to form spheroidal BCP particles, including ellipsoids and oblates. For example, pioneering work from Hawker *et al.* used CTAB/CTAB–OH as dual surfactants to form ellipsoidal particles of polystyrene-*block*-poly(2-vinyl pyridine) (PS-*b*-P2VP), driven by the selective affinity of CTAB and CTAB–OH for the PS and P2VP blocks, respectively.[25] Based on the preferential interaction of CTAB–OH and P2VP *via* hydrogen bonding of the hydroxyl group with pyridine units, other similar surfactants were designed and applied for controlling the particle shape in the scope of BCPs containing P2VP or poly(4-vinylpyridine) (P4VP) blocks.[26–28]

[a]*Department of Chemical and Biomolecular Engineering, Korea Advanced Institute of Science and Technology (KAIST), Daejeon 34141, Republic of Korea. E-mail: bumjoonkim@kaist.ac.kr*

[b]*Department of Materials Science and Engineering, Soongsil University, Seoul 06978, Republic of Korea. E-mail: jshin@ssu.ac.kr*

† Electronic supplementary information (ESI) available: Double bond conversion, SEM and TEM images of the particles. See DOI: https://doi.org/10.1039/d4py00524d

‡ These authors contributed equally to this work.

However, the applicability of this strategy is limited to BCPs consisting of highly immiscible blocks (*i.e.*, high Flory–Huggins interaction parameter (χ)). Thus, examples of using a mixture of surfactants to non-selective low-χ BCPs are rarely reported.[29] Alternatively, the shape transition of low-χ BCP particles has been achieved by carefully controlling the solvent evaporation rate from BCP-containing emulsions. However, as anisotropic particles in these works are kinetically controlled, and the obtained shapes and morphologies are metastable.[30–34]

Polystyrene-*block*-polybutadiene (PS-*b*-PB) represents an example of low-χ BCPs, which can serve as an important building block for generating self-assembled nanomaterials, including the PS-*b*-PB-*b*-PS (SBS) thermoplastic elastomers that are extensively utilized across various industries.[35–37] In particular, chemical modification of PB has been utilized to tune the physicochemical properties of PS-*b*-PB BCPs in bulk or thin films,[38–40] as the diene group in PB can be easily functionalized with various chemistries.[41–44] Nevertheless, there has been less focus on establishing a reliable platform to fabricate shape-transforming PS-*b*-PB particles *via* diene group modification, potentially due to difficulty in particle shape transition through chemical modification. For example, thiol–ene chemistry[45,46] was employed to modify PS-*b*-PB particles by selectively conjugating functional molecules on the PB block, however, the resulting shape transition was minimal or incomplete.[47,48] Also, side reactions (*e.g.* bimolecular termination) can occur under typical thiol–ene reaction conditions, which can significantly hinder the particle shape transformation.[49] In this regard, an effective chemical modification process should be developed to fabricate responsive PS-*b*-PB particles with controllable shapes and internal structures, considering the commercial significance of PS-*b*-PB BCPs.

Herein, we report shape transitions of PS-*b*-PB BCP particles based on selective I_2-doping in PB domains. The spherical BCP particles are first prepared from an evaporative oil-in-water emulsion, followed by reconstructing colloidal particles using dichloromethane/iodine (DCM/I_2) vapor annealing. During this process, I_2 selectively reacts with the double bonds in PB domains and modulates the interfacial tension, allowing for the shape transition of BCP particles from spheres into oblate and prolate spheroids. Longer reaction time leads to a higher degree of double bond conversion into iodine-doped cation radicals, which is consistent with the gradual shape transformation of BCP spheres into oblates and prolate ellipsoids as a function of reaction time. We revealed that shape transition is driven by the decrease in interfacial tension between the PB domain and surroundings, achieving a neutral interaction of PS/surrounding and PB/surrounding at a certain level of I_2 doping. The versatility of our method is demonstrated by applying the same strategy to PS-*b*-P4VP BCPs with various molecular weight and volume fractions. For all BCPs, the I_2-doping has successfully demonstrated the shape transformation of spherical particles into oblates or prolate ellipsoids. Finally, I_2-doped ellipsoidal particles exhibit excellent photothermal behavior compared to pristine spherical particles, highlighting the potential application of chemically modified BCP particles.

Experimental section

Materials

PS_{35k}-*b*-PB_{11k} (subscripts indicate the number-average molecular weight (M_n), polydispersity index ($Đ$) = 1.12), PS_{34k}-*b*-PB_{25k}, ($Đ$ = 1.12), PS_{10k}-*b*-$P4VP_{10k}$ ($Đ$ = 1.08), PS_{15k}-*b*-$P4VP_{7k}$ ($Đ$ = 1.18), PS_{24k}-*b*-$P4VP_{51k}$ ($Đ$ = 1.15), PS_{30k} ($Đ$ = 1.15), PB_{11k} ($Đ$ = 1.12) were purchased from Polymer Source, Inc. Cetyltrimethylammonium bromide (CTAB) and iodine (I_2) were purchased from Sigma-Aldrich and used without further purification.

Preparation of spherical BCP particles

A DCM solution containing PS-*b*-PB or PS-*b*-P4VP (10 mg mL^{-1}) was prepared and stirred at room temperature for 12 h. Then, the polymer solution (0.1 mL) was emulsified with 1 mL of surfactant-containing aqueous solution (10 mg mL^{-1}, CTAB) by vortexing at 10 000 rpm for 1 min. Subsequently, DCM was evaporated at room temperature for 24 h. The residual surfactants were removed by repeated centrifugation at 12 000 rpm and redispersion in water for 3 times, and the resulting particles were used for further characterization.

Iodine-mediated modification of BCP particles

0.5 mL suspensions of BCP spheres were re-dispersed into a surfactant-containing aqueous solution (1 mg mL^{-1}, CTAB). The particle suspension was transferred into a 4 mL vial, which was placed inside a larger 20 mL vial containing 2 mL of DCM/I_2 (2 mg mL^{-1}) solution at the bottom. The 20 mL vial was sealed and kept at 40 °C to allow the reaction to proceed, where the presence of DCM vapors annealed the BCP particles to undergo shape restructuring. After annealing for a predetermined time, the 4 mL vial containing the particles was taken out and kept in the open air to evaporate residual DCM/I_2.

Characterization

Scanning electron microscopy (SEM, Magellan 400), transmission electron microscopy (TEM, Tecnai F20, 200 kV), and field-emission transmission electron microscopy (FE-TEM, Talos F200X) were used to observe the surface and internal structure of the BCP particles. SEM samples were prepared by drop-casting the BCP particle suspension on the silicon wafer. For TEM samples, 10 μL BCP particle suspension was transferred to the carbon-supported grid and dried in air. The PB domain was stained prior to TEM imaging by adding diluted OsO_4 solution (0.2 wt%, 60 μL) to the BCP particle suspension (0.5 mL) after which the solution turned dark. For PS-*b*-P4VP particles, the carbon-supported grid with BCP particles was subjected to iodine vapor to selectively stain the P4VP domain. Fourier-transform infrared spectroscopy (FT-IR) measurement was performed on a Nicolet iS500 FT-IR spectrometer (Thermo

Fisher Scientific Instrument). FT-IR samples were prepared by concentrating the particles by centrifugation, followed by drying in a vacuum at 40 °C. Proton nuclear magnetic resonance (^{1}H NMR) spectra were obtained from a Bruker AVANCE III HD instrument at 400 MHz using $CDCl_3$ as solvent. A pendant drop method was performed to analyze the interfacial tensions between the polymer solution (*i.e.*, PS_{30k}, PB_{11k} in DCM, 10 mg mL^{-1}) and the aqueous surfactant solution (*i.e.*, CTAB, 10 mg mL^{-1} in water). The pendant drop images were taken with a CCD camera (WAT-902H Ultimate, Watec) and were analyzed by the MATLAB program to determine the interfacial tension values.

Results and discussion

Scheme 1 shows our overall experimental system. First, spherical BCP particles are prepared by emulsifying a DCM solution containing PS-*b*-PB BCPs (10 mg mL^{-1}) with an aqueous solution containing CTAB surfactant (10 mg mL^{-1}). After evaporation of DCM, the spherical particles are obtained in which coiled PB cylinders and concentric lamellar layers are formed inside the particles for PS_{35k}-*b*-PB_{11k} and PS_{34k}-*b*-PB_{25k}, respectively. Then, the obtained BCP spheres are exposed to DCM/I_2 vapors for two purposes: I_2 vapors react with PB domains, and DCM vapors make the BCP chains mobile to allow the shape transitions of the spherical particles.[22,50–53] After the reaction, the polarity of I_2-doped PB chains increases, leading to the reduced interfacial tension between the modified PB domain and the aqueous surrounding. Accordingly, when the PS blocks and modified PB blocks exhibit comparable affinities to their surroundings, neutral interfacial interaction is attained to allow the transformation of spherical particles into oblate and prolate ellipsoids.

Fig. 1a shows the reaction scheme for the I_2-doping of PS-*b*-PB BCPs. I_2 serves as a strong oxidant undergoing reduction to I^- or I_3^- while generating cation radicals in C=C double bonds of the PB segment.[54,55] In contrast, PS blocks have no reactivity toward the I_2 molecules. Fig. 1b and c shows the shape and internal morphology of as-prepared spherical PS_{35k}-*b*-PB_{11k} particles. As CTAB is a typical PS-selective surfactant,[11,25] outermost layer consists of PS domains while the cylindrical PB domains are internally coiled within the spherical confinement. After treating these particles with DCM/I_2 vapors for 12 hours, the particles were transformed into well-defined oblates with hexagonally packed PB cylinders embedded in the PS matrix (Fig. 1d and e). Additionally, the increase in the aspect ratio (AR) of oblate particles to 1.29 after 12 h of reaction reflects the formation of anisotropic BCP particles (Table S1†). By performing the elemental mapping analysis of the dark-field STEM image, the hexagonal arrays of I_2 clearly show (inset in Fig. 1e) that the I_2 doping proceeded solely in PB chains while PS remained intact.

To better observe the shape transition process, the structural evolution of the particle shape and internal morphology of PS_{35k}-*b*-PB_{11k} was monitored as a function of reaction times (Fig. 2). First, the pristine spherical PS_{35k}-*b*-PB_{11k} particles

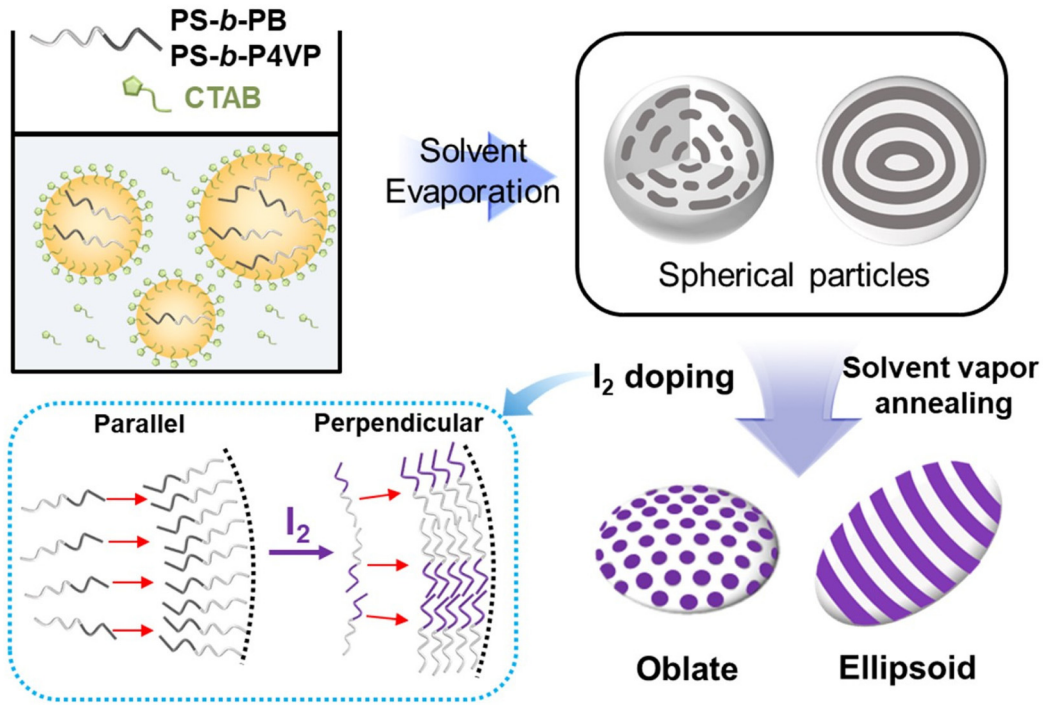

Scheme 1 Experimental system showing the generation of spherical BCP particles *via* emulsion-solvent evaporation, followed by I_2 doping to transform spherical BCP particles into oblates and ellipsoids.

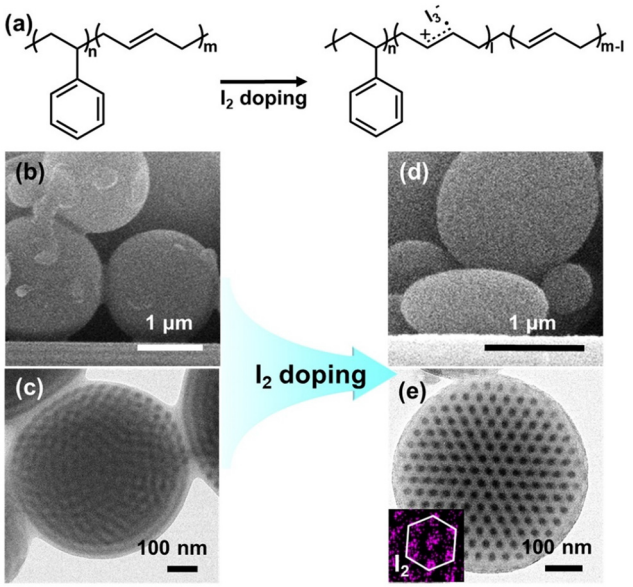

Fig. 1 (a) Reaction scheme for I_2 doping of PS-*b*-PB. (b and c) Side view SEM and top TEM images of pristine PS_{35k}-*b*-PB_{11k} spherical particles; (d and e) side view SEM and top TEM images of PS_{35k}-*b*-PB_{11k} oblate particles after I_2 doping for 12 h. Inset in (e) shows the elemental mapping of I_2 in the oblate particles. PB domains appear dark due to OsO_4 staining.

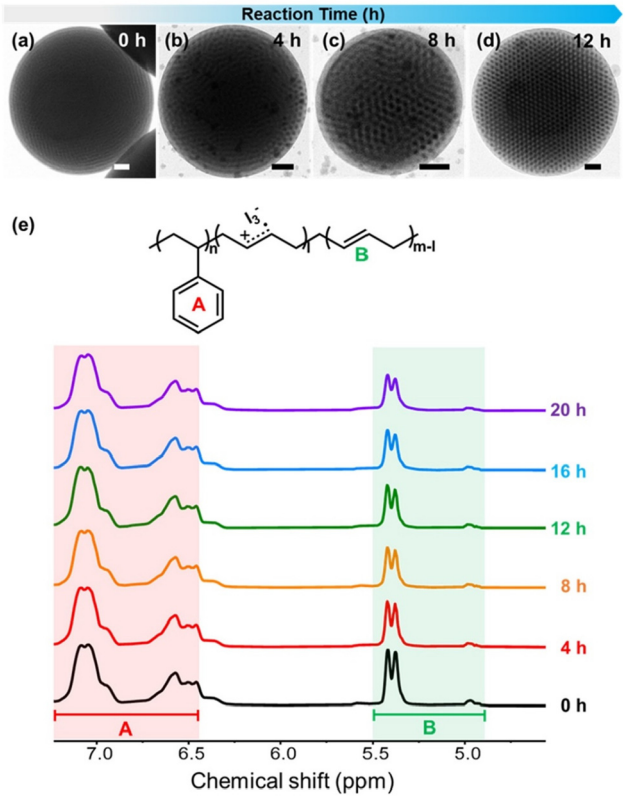

Fig. 2 (a–d) TEM images showing the morphology transitions from PS_{35k}-*b*-PB_{11k} spherical particles to oblates at different reaction times in DCM/I_2. Scale bars are 100 nm. (e) ^{1}H NMR spectra of PS-*b*-PB after reacting with I_2 for different time. The aromatic signals between 6.4 ppm and 7.2 ppm are highlighted in red (A) while vinylic protons in PB between 4.9 ppm and 5.5 ppm are highlighted in green (B).

with coiled PB cylinders having a domain spacing (D) of 33 ± 2.3 nm were initially formed (Fig. 2a). After exposing this particle to DCM/I_2 vapors for 4 h, hexagonally packed structures started to form at the surface of the BCP particle, indicating that the PB cylinders are perpendicularly oriented to the particle surface (Fig. 2b). Such a feature became more prominent after 8 h of reaction, where perpendicularly oriented cylindrical PB domains span throughout the particle (Fig. 2c). After 12 h of reaction, complete transformation to oblate particles (D = 39 ± 1.5 nm) with well-organized, hexagonally-packed PB cylinders was observed (Fig. 2d). We attribute the gradual increase of D with an increasing reaction time to the swollen PB domains by solvent and the addition of I_2 molecules within the modified PB domains.

The shape transition process from BCP spheres to oblates is further investigated by obtaining statistics that show the percentage of oblate particles in the particle batch as a function of reaction time (Fig. S1†). For the particles that reacted for 4 h and 8 h, 11% and 36% of oblate particles were observed, respectively (Fig. S1a–c†). The percentage of oblate particles was significantly increased to 85% at the reaction time of 12 h (Fig. S1d†). At longer reaction times of 16 and 20 h, slight increases in the percentage of oblate particles (88% and 89%, Fig. S1e and f†) indicate that the near-complete transformation into oblate particles can be attained after 12 h of reaction time. Similarly, the shape transition process of the lamellar forming PS_{34k}-*b*-PB_{25k} particles was monitored at different reaction times (Fig. S2 and S3†). First, the pristine PS_{34k}-*b*-PB_{25k} forms onion-like spherical particles with PS as the outermost layer (Fig. S2a†). After 4 h and 8 h of exposure to iodine vapors, particles with an intermediate morphology between onion and ellipsoid were observed, indicating a mixed orientation of parallel and perpendicular domains relative to the particle surface (Fig. S2b and c†). At 12 h of reaction, the particles were fully transformed into elongated ellipsoids with well-defined lamellae structures (Fig. S2d†). The percentage of PS_{34k}-*b*-PB_{25k} particles transition from spheres to ellipsoidal shapes was presented in Fig. S3† as a function of reaction time.

We quantitatively evaluated the degree of reaction as a function of reaction time by calculating the conversion of double bonds (R) in PB chains from ^{1}H NMR spectra (Fig. 2e). In detail, the integration values of vinylic protons in PB (4.9–5.5 ppm) compared to that of aromatic signals (6.4–7.2 ppm) from intact PS chains were used to calculate the R values as a function of reaction time (Table S2†).[47] Specifically, R increased gradually from 0 to 10.3, 15.2 and 17.9% after 4, 8, and 12 h of reaction time, respectively. As the majority of particles turned to oblates after 12 h of reaction time, we speculate that the critical conversion of double bonds by I_2 to induce the switching of BCP orientation is around 17%. Further extension of the reaction time to 16 and 20 h led

to the increase of R to 22% and 31%, respectively, although the oblate shape of the particle is maintained at these reaction times (Fig. S1†). A similar conclusion can be made by comparing the FT-IR spectra of pristine spherical and oblate particles obtained after the 20 h reaction. As shown in Fig. S4,† the decrease in peak intensity at 908 cm^{-1}, which corresponds to the alkene =C–H bending peak, indicates that the double bonds in PB reacted with the I_2 molecules.

The interfacial interaction of modified PB domains plays a key role in obtaining oblate BCP particles.[6,9,25] The interfacial tensions (γ) between each polymer block and the aqueous surroundings were examined as a function of reaction time. The difference in the interfacial tension between PS and PB ($\Delta\gamma = \gamma_{PB} - \gamma_{PS}$) is plotted in Fig. 3. The measured values of γ between the PS block and the aqueous surroundings were kept nearly constant ($\gamma_{PS} \sim 4.12$ mN m^{-1}) for all reaction times while that of the PB block and the surroundings (γ_{PB}) gradually decreased from 4.95 to 3.96 mN m^{-1} after 20 h of reaction time (Table S3†). The constant γ_{PS} value is consistent with the intact PS block during the reaction as observed in the ^{1}H NMR spectra, while the decrease in γ_{PB} can be attributed to the enhanced polarity of I_2-doped PB domains.[54] Notably, the $\Delta\gamma$ value can serve as an indicator of neutral interfacial interactions, as the shape transformation of the BCP particles is expected to occur at the neutral condition of $\Delta\gamma \sim 0$. Although PS-*b*-PBs are typical low-χ BCPs,[56] a $\Delta\gamma$ value of 0.83 before I_2 doping indicated interfacial selectivity toward the PS block in the pristine spherical BCP particles, positioning the PS as the outermost layer. At a short reaction time of 4 and 8 h, $\Delta\gamma$ decreased to 0.52 and 0.24, respectively. Further extension of the reaction time to 12 h led to the $\Delta\gamma$ close to zero ($\Delta\gamma = 0.01$), indicating a neutralized interfacial interaction of PS and PB to surroundings. This is in good accordance with the emergence of oblate and prolate particles as observed by the electron microscopy tools.

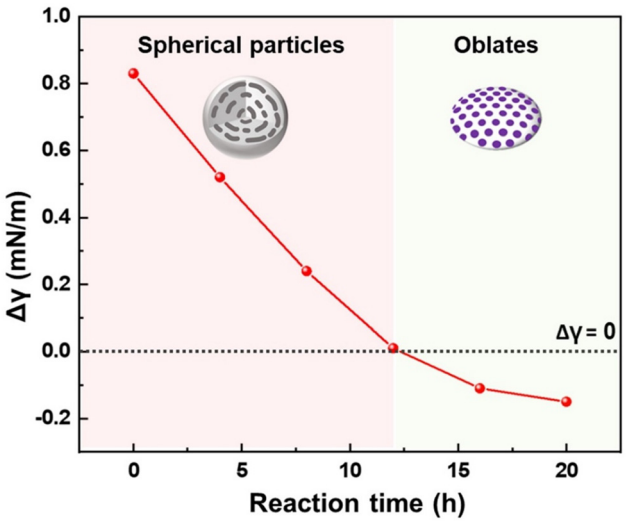

Fig. 3 Interfacial tension difference ($\Delta\gamma = \gamma_{PB} - \gamma_{PS}$) as a function of reaction time. The dashed line indicates the $\Delta\gamma = 0$.

The versatility of I_2-doping induced shape transition of BCP particles is further demonstrated by using PS-*b*-P4VP BCP particles with a wide range of volume fractions. While it is well-known that I_2 molecules can physically bind to pyridine group (Pyr*I_2),[57–59] I_2 can be further dissociated into ions ($PyrI^+ + I^-$) and form stronger bond with P4VP chains (Scheme S1†), similar to the oxidation of diene group in PB.[60,61] Fig. 4 shows the successful shape transformations of PS_{15k}-*b*-$P4VP_{7k}$, PS_{10k}-*b*-$P4VP_{10k}$, and PS_{24k}-*b*-$P4VP_{51k}$ spheres into spheroids upon reacting with I_2. Additionally, I_2 doped PS-*b*-P4VP particles exhibited long-term stability (Fig. S5†), supporting the formation of strong ionic complex between iodine and P4VP. For PS_{15k}-*b*-$P4VP_{7k}$, pristine spherical particles with coiled P4VP cylinders were formed (Fig. 4a and b). After reacting with I_2 for 12 h, the spheres transitioned into oblate particles with hexagonally packed cylinders having increased D from 21 ± 1.7 nm to 30 ± 2.4 nm while AR increased from 1.0 to 2.1. For PS_{10k}-*b*-$P4VP_{10k}$, onion-like particles transformed into ellipsoidal particles with axially stacked lamellae (Fig. 4e–h) having increased D from 20 ± 1.6 nm to 28 ± 2.1 nm and increased AR from 1.0 to 1.9. Finally, the PS_{24k}-*b*-$P4VP_{51k}$ spherical particles having coiled PS cylinders (D = 60 ± 2.2 nm) transformed into oblate particles with perpendicular PS cylinders (D = 67 ± 3.1 nm) after the I_2 reaction, and the average AR was significantly increased to 3.7 (Fig. 4(i–l)). We summarized the D and AR values of PS-*b*-P4VP particles before and after the I_2 reaction in Table S4.† The increase in D can be attributed to the (i) swelling of ionized P4VP blocks by aqueous surroundings[62–64] and (ii) the increase in interaction parameter (χ) between the PS and the modified P4VP block.[65,66] Overall, I_2 doping of P4VP blocks successfully modulated the interfacial interaction between each block and the surroundings, leading to the formation of well-defined anisotropic PS-*b*-P4VP particles (*e.g.*, oblate or ellipsoid) similar to the shape transition observed in PS-*b*-PB BCP particles.

We examined the photothermal behavior of I_2-doped non-spherical BCP particles as the I_2-doping can lead to the materials for higher efficiency in light absorption.[67,68] The color of the nonspherical PS_{34k}-*b*-PB_{25k} particles was changed from white to black after the reaction with I_2 (Fig. S6†), and the photothermal behaviors were evaluated by recording the temperature change under the irradiation of an 808 nm laser source (Fig. 5). A rapid heating of the suspension containing I_2-doped particles (1.0 mg mL^{-1}) was visualized in the IR thermograph, particularly at the bottom of the tube where the particles are concentrated (Fig. 5a). Also, I_2-doped ellipsoidal particles after IR heating retained their original shape and internal structure, indicating that the photothermal particles are stable in the observed range of temperatures (Fig. S7†). Additionally, the temperature change of the I_2-doped particles was compared with various control samples (Fig. 5b). The suspension of pristine spheres and distilled water showed no change in temperature (17.4 °C, ΔT < 2.0 °C) until 900 s of irradiation. In contrast, the temperature of the suspension containing 0.4 and 1.0 mg mL^{-1} of I_2-doped particles increased to 48.6 °C and 71.3 °C at 900 s, respectively. Overall,

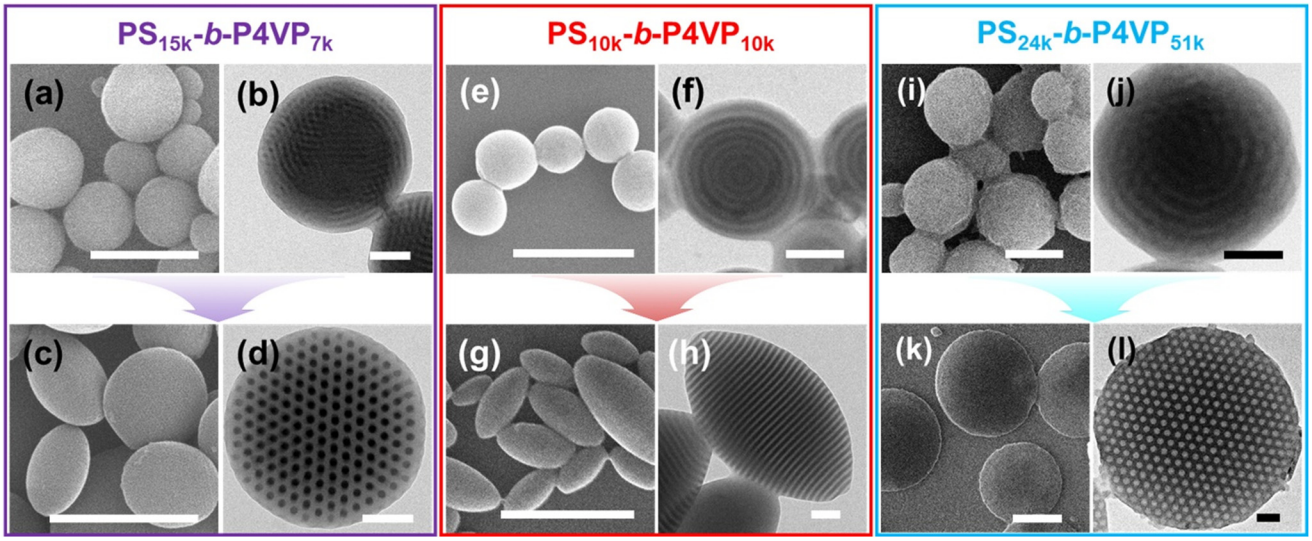

Fig. 4 SEM and TEM images of (a and b) PS_{15k}-*b*-$P4VP_{7k}$ spherical particles before I_2 doping and (c and d) oblate particles after I_2 doping. SEM and TEM images of (e and f) PS_{10k}-*b*-$P4VP_{10k}$ spherical particles before I_2 doping and (g and h) prolate ellipsoids after I_2 doping. SEM and TEM images of (i and j) PS_{24k}-*b*-$P4VP_{51k}$ spherical particles before I_2 doping and (k and l) inverse oblate particles after I_2 doping. Scale bars in SEM images are 1 μm and TEM images are 100 nm.

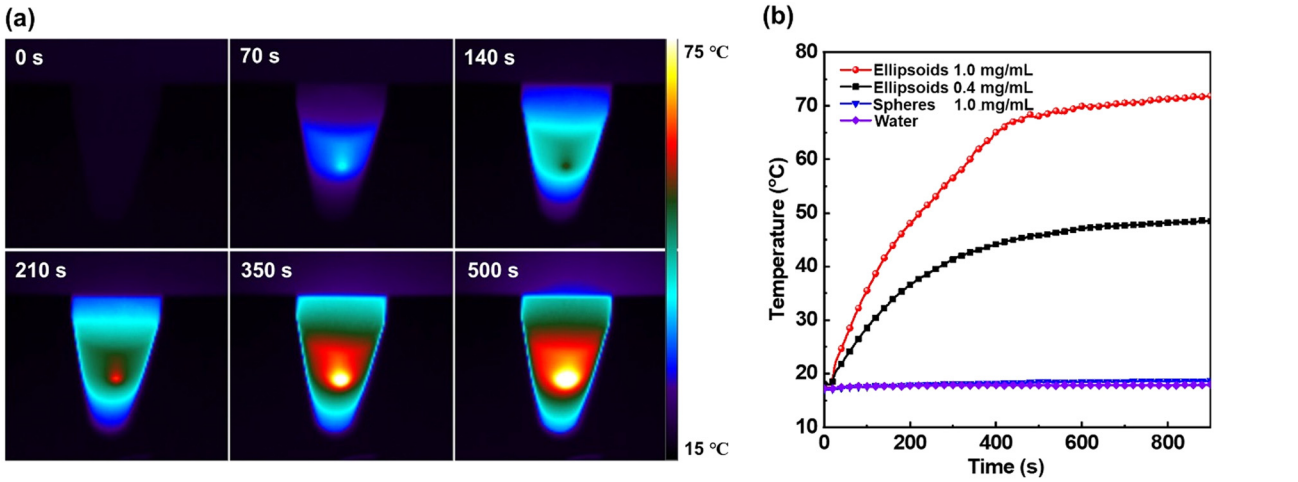

Fig. 5 (a) IR thermal photographs of the suspension of I_2-doped ellipsoidal particles (1.0 mg mL^{-1}) as a function of irradiation times. (b) A time-dependent temperature change of suspensions of pristine (blue line) and I_2-doped (red and black lines) PS-*b*-PB particles. For a comparison, distilled water was also tested. The suspension was irradiated with an 808 nm laser at an intensity of 1.0 W cm^{-2}.

facile functionalization of PS-*b*-PB particles with I_2 allowed the generation of nonspherical shapes, and the resulting I_2-doped particles showed excellent photothermal effect.

Conclusions

In summary, we have developed a facile strategy to induce the shape transitions of spherical PS-*b*-PB BCP particles into anisotropic shapes using the I_2-mediated reaction in combination with the solvent vapor annealing process. The I_2 molecules selectively reacted with the double bonds in PB chains to form cation radicals, and the degree of I_2 doping can be tuned by the reaction time. The incorporation of I_2 enhanced the polarity of the modified PB blocks to decrease interfacial tension with the aqueous surroundings. Accordingly, neutralization of the interfacial interaction switched the orientation of BCP domains perpendicular to the surface, allowing the shape transformation from spherical BCP particles into oblates or ellipsoids. Furthermore, the versatility of our strategy was demonstrated by applying it to the PS-*b*-P4VP BCPs with various molecular weight and volume fractions. Finally, I_2-doped ellipsoidal particles exhibited excellent photothermal behavior as compared to the pristine spherical particles, high-

lighting the potential application of these particles as a photothermal agent.

Data availability

The data supporting this article have been included as part of the ESI.†

Conflicts of interest

The authors declare no competing financial interest.

Acknowledgements

This research was supported by the Korea Research Foundation Grant, funded by the Korean Government (RS-2023-00244864). This work was supported by Korea Institute of Energy Technology Evaluation and Planning (KETEP) grant funded by the Korea government (MOTIE) (20214000000650).

References

1 S. Mitragotri and J. Lahann, *Nat. Mater.*, 2009, **8**, 15–23.
2 P. J. Yunker, T. Still, M. A. Lohr and A. G. Yodh, *Nature*, 2011, **476**, 308–311.
3 Q. He, K. H. Ku, H. Vijayamohanan, B. J. Kim and T. M. Swager, *J. Am. Chem. Soc.*, 2020, **142**, 10424–10430.
4 J. A. Champion and S. Mitragotri, *Proc. Natl. Acad. Sci. U. S. A.*, 2006, **103**, 4930–4934.
5 N. Yan, Y. Zhu and W. Jiang, *Chem. Commun.*, 2018, **54**, 13183–13195.
6 K. H. Ku, J. M. Shin, H. Yun, G.-R. Yi, S. G. Jang and B. J. Kim, *Adv. Funct. Mater.*, 2018, **28**, 1802961.
7 C. K. Wong, X. Qiang, A. H. Müller and A. H. Gröschel, *Prog. Polym. Sci.*, 2020, **102**, 101211.
8 M. Peng, D. Hu, X. Chang and Y. Zhu, *J. Phys. Chem. B*, 2022, **126**, 9435–9442.
9 J. J. Shin, E. J. Kim, K. H. Ku, Y. J. Lee, C. J. Hawker and B. J. Kim, *ACS Macro Lett.*, 2020, **9**, 306–317.
10 K. H. Ku, Y. J. Lee, Y. Kim and B. J. Kim, *Macromolecules*, 2019, **52**, 1150–1157.
11 S. G. Jang, D. J. Audus, D. Klinger, D. V. Krogstad, B. J. Kim, A. Cameron, S. W. Kim, K. T. Delaney, S. M. Hur, K. L. Killops, G. H. Fredrickson, E. J. Kramer and C. J. Hawker, *J. Am. Chem. Soc.*, 2013, **135**, 6649–6657.
12 J. Lee, K. H. Ku, M. Kim, J. M. Shin, J. Han, C. H. Park, G.-R. Yi, S. G. Jang and B. J. Kim, *Adv. Mater.*, 2017, **29**, 1700608.
13 J. Kim, H. Yun, Y. J. Lee, J. Lee, S. H. Kim, K. H. Ku and B. J. Kim, *J. Am. Chem. Soc.*, 2021, **143**, 13333–13341.
14 J. Lee, K. H. Ku, J. Kim, Y. J. Lee, S. G. Jang and B. J. Kim, *J. Am. Chem. Soc.*, 2019, **141**, 15348–15355.
15 D. Hu, X. Chang, Y. Xu, Q. Yu and Y. Zhu, *ACS Macro Lett.*, 2021, **10**, 914–920.
16 J. Lee, K. H. Ku, C. H. Park, Y. J. Lee, H. Yun and B. J. Kim, *ACS Nano*, 2019, **13**, 4230–4237.
17 J. Kim, J. Park, K. Jung, E. J. Kim, Z. Tan, M. Xu, Y. J. Lee, K. H. Ku and B. J. Kim, *ACS Nano*, 2024, **18**, 8180–8189.
18 S. H. Kwon, M. Xu, J. Kim, E. J. Kim, Y. J. Lee, S. G. Jang, H. Yun and B. J. Kim, *Chem. Mater.*, 2021, **33**, 9769–9779.
19 Y. Wang, D. Hu, X. Chang and Y. Zhu, *Macromolecules*, 2022, **55**, 6211–6219.
20 R. Deng, J. Xu, G.-R. Yi, J. W. Kim and J. Zhu, *Adv. Funct. Mater.*, 2021, **31**, 2008169.
21 C. Lu and M. W. Urban, *Prog. Polym. Sci.*, 2018, **78**, 24–46.
22 J. M. Shin, Y. J. Lee, M. Kim, K. H. Ku, J. Lee, Y. Kim, H. Yun, K. Liao, C. J. Hawker and B. J. Kim, *Chem. Mater.*, 2019, **31**, 1066–1074.
23 K. H. Ku, J. H. Ryu, J. Kim, H. Yun, C. Nam, J. M. Shin, Y. Kim, S. G. Jang, W. B. Lee and B. J. Kim, *Chem. Mater.*, 2018, **30**, 8669–8678.
24 J. Xu, K. Wang, J. Li, H. Zhou, X. Xie and J. Zhu, *Macromolecules*, 2015, **48**, 2628–2636.
25 D. Klinger, C. X. Wang, L. A. Connal, D. J. Audus, S. G. Jang, S. Kraemer, K. L. Killops, G. H. Fredrickson, E. J. Kramer and C. J. Hawker, *Angew. Chem., Int. Ed.*, 2014, **53**, 7018–7022.
26 R. Deng, F. Liang, W. Li, Z. Yang and J. Zhu, *Macromolecules*, 2013, **46**, 7012–7017.
27 B. Schmidt, J. Elbert, D. Scheid, C. J. Hawker, D. Klinger and M. Gallei, *ACS Macro Lett.*, 2015, **4**, 731–735.
28 C. Chen, Z. Xiao and L. A. Connal, *Aust. J. Chem.*, 2016, **69**, 741–745.
29 S. J. Jeon, G. R. Yi and S. M. Yang, *Adv. Mater.*, 2008, **20**, 4103–4108.
30 J. M. Shin, Y. Kim, H. Yun, G. R. Yi and B. J. Kim, *ACS Nano*, 2017, **11**, 2133–2142.
31 J. M. Shin, Y. J. Kim, K. H. Ku, Y. J. Lee, E. J. Kim, G. R. Yi and B. J. Kim, *Chem. Mater.*, 2018, **30**, 6277–6288.
32 T. Higuchi, A. Tajima, K. Motoyoshi, H. Yabu and M. Shimomura, *Angew. Chem., Int. Ed.*, 2008, **47**, 8044–8046.
33 H. Yabu, T. Higuchi and M. Shimomura, *Adv. Mater.*, 2005, **17**, 2062–2065.
34 H. Li, X. Mao, H. Wang, Z. Geng, B. Xiong, L. Zhang, S. Liu, J. Xu and J. Zhu, *Macromolecules*, 2020, **53**, 4214–4223.
35 L. S. Flosenzier and J. M. Torkelson, *Macromolecules*, 1992, **25**, 735–742.
36 N. R. Legge, G. Holden and H. E. Schroeder, *Thermoplastic Elastomers: A Comprehensive Review*, Hanser, NewYork, 1987.
37 Kraton thermoplastic rubber. Technical Bulletin, SC: 971-87, Shell Chemical Company.
38 H. Feng, M. Dolejsi, N. Zhu, P. J. Griffin, G. S. W. Craig, W. Chen, S. J. Rowan and P. F. Nealey, *Adv. Funct. Mater.*, 2022, **32**, 2206836.

39 B. Sutisna, G. Polymeropoulos, V. Musteata, R. Sougrat, D. M. Smilgies, K. V. Peinemann, N. Hadjichristidis and S. P. Nunes, *Small*, 2018, **14**, e1701885.
40 H. Fang, X. Gao, F. Zhang, W. Zhou, G. Qi, K. Song, S. Cheng, Y. Ding and H. H. Winter, *Macromolecules*, 2022, **55**, 10900–10911.
41 C. M. Geiselhart, J. T. Offenloch, H. Mutlu and C. Barner-Kowollik, *ACS Macro Lett.*, 2016, **5**, 1146–1151.
42 A. Zhang and L. Chao, *Eur. Polym. J.*, 2003, **39**, 1291–1295.
43 R. Pandit, J. Giri, G. H. Michler, R. Lach, W. Grellmann, B. Youssef, J. M. Saiter and R. Adhikari, *Macromol. Symp.*, 2012, **315**, 152–159.
44 Y. Ren, T. P. Lodge and M. A. Hillmyer, *Macromolecules*, 2002, **35**, 3889–3894.
45 D. P. Nair, M. Podgórski, S. Chatani, T. Gong, W. Xi, C. R. Fenoli and C. N. Bowman, *Chem. Mater.*, 2014, **26**, 724–744.
46 C. E. Hoyle and C. N. Bowman, *Angew. Chem., Int. Ed.*, 2010, **49**, 1540–1573.
47 J. J. Shin, *Polymers*, 2020, **12**, 2804.
48 D. Varadharajan, H. Turgut, J. Lahann, H. Yabu and G. Delaittre, *Adv. Funct. Mater.*, 2018, **28**, 1800846.
49 S. P. S. Koo, M. M. Stamenović, R. A. Prasath, A. J. Inglis, F. E. Du Prez, C. Barner-Kowollik, W. Van Camp and T. Junker, *J. Polym. Sci., Part A: Polym. Chem.*, 2010, **48**, 1699–1713.
50 L. Navarro, A. F. Thunemann and D. Klinger, *ACS Macro Lett.*, 2022, **11**, 329–335.
51 X. Mao, H. Li, J. Kim, S. Deng, R. Deng, B. J. Kim and J. Zhu, *Nano Res.*, 2021, **14**, 4644–4649.
52 L. Li, K. Matsunaga, J. Zhu, T. Higuchi, H. Yabu, M. Shimomura, H. Jinnai, R. C. Hayward and T. P. Russell, *Macromolecules*, 2010, **43**, 7807–7812.
53 X. Qiang, X. Dai, A. Steinhaus and A. H. Gröschel, *ACS Macro Lett.*, 2019, **8**, 1654–1659.
54 R. Li, Z. Wang, X. Tao, J. Jia, X. Lian and Y. Wang, *ACS Macro Lett.*, 2020, **9**, 985–990.
55 R. Li, Z. Wang and Y. Wang, *Innovation*, 2021, **2**, 100095.
56 G. Kim and M. Libera, *Macromolecules*, 1998, **31**, 2569–2577.
57 X. Zheng, M. Ren, H. Wang, H. Wang, Z. Geng, J. Xu, R. Deng, S. Chen, W. H. Binder and J. Zhu, *Small*, 2021, **17**, 2007570.
58 G. Quintieri, M. Saccone, M. Spengler, M. Giese and A. H. Gröschel, *Nanomaterials*, 2018, **8**, 1029.
59 R. Milani, N. Houbenov, F. Fernandez-Palacio, G. Cavallo, A. Luzio, J. Haataja, G. Giancane, M. Saccone, A. Priimagi, P. Metrangolo and O. Ikkala, *Chem*, 2017, **2**, 417–426.
60 H. T. Nguyen, D. D. Nguyen and J. Spanget-Larsen, *Chem. Phys. Lett.*, 2019, **716**, 119–125.
61 T. Tassaing and M. Besnard, *J. Phys. Chem. A*, 1997, **101**, 2803–2808.
62 A. Hanisch, A. H. Gröschel, M. Förtsch, M. Drechsler, H. Jinnai, T. M. Ruhland, F. H. Schacher and A. H. E. Müller, *ACS Nano*, 2013, **7**, 4030–4041.
63 Z. Tan, E. J. Kim, T. N.-L. Phan, J. Kim, J. J. Shin, K. H. Ku and B. J. Kim, *Macromolecules*, 2022, **55**, 9972–9979.
64 S. Lee, J. J. Shin, K. H. Ku, Y. J. Lee, S. G. Jang, H. Yun and B. J. Kim, *Macromolecules*, 2020, **53**, 7198–7206.
65 A. Semenov, *Zh. Eksp. Teor. Fiz.*, 1985, **88**, 1242–1256.
66 F. S. Bates and G. H. Fredrickson, *Annu. Rev. Phys. Chem.*, 1990, **41**, 525–557.
67 Z. Wang, X. Lian, R. Li, X. Tao and Y. Wang, *Chem. – Eur. J.*, 2019, **25**, 13811–13815.
68 R. Li, Z. Wang, P. Han, Y. He, X. Zhang and Y. Wang, *Chem. – Eur. J.*, 2017, **23**, 17889–17893.